Controllable 1,4-Palladium Aryl to Aryl Migration in Fused Systems Application to the Synthesis of Azaborole Multihelicenes

Felix Full, Albert Artigas, Kevin Wiegand, Daniel Volland, Klaudia Szkodzińska, Yoann Coquerel, Agnieszka Nowak-Król

Controllable 1,4-Palladium Aryl to Aryl Migration in Fused Systems – Application to the Synthesis of Azaborole Multihelicenes

Felix Full,[†] Albert Artigas,[‖] Kevin Wiegand,[†] Daniel Volland,[†] Klaudia Szkodzińska,[†] Yoann Coquerel,[‡] Agnieszka Nowak-Król[†,*]

[†]*Institut für Anorganische Chemie and Institute for Sustainable Chemistry & Catalysis with Boron, Universität Würzburg, Am Hubland, Würzburg, Germany*

[‖]*Facultat de Ciències, Campus Montilivi, Carrer de Maria Aurèlia Capmany i Farnès, 69, Girona, Catalunya, Spain*

[‡]*Aix Marseille Univ, CNRS, Centrale Med, ISM2, Marseille, France*

Keywords: Acetate, Aromaticity, Azaboroles, Chiroptical Properties, Fluorescence, Helicenes, Miyaura Borylation, Multihelicenes 1,4-Palladium Migration

ABSTRACT: Herein, we report the first 1,4-Pd aryl to aryl migration/Miyaura borylation tandem reaction in fused systems. The Pd shift occurred in the bay region of the dibenzo[*g*,*p*]chrysene building blocks, giving rise to a thermodynamically controlled mixture of 1,8- and 1,9-borylated compounds that allowed the preparation of regioisomeric azaborole multihelicenes from the same starting material. The outcome of this synthesis can be controlled by the choice of reaction conditions, allowing the migration process to be turned off in the absence of an acetate additive and the target multiheterohelicenes to be prepared in a regioselective manner. The target compounds show bright green fluorescence in dichloromethane with emission quantum yields (Φ) of up to 0.29, $|g_{lum}|$ values up to 2.7×10^{-3}, and green or green-yellow emission in the solid state, reaching Φ of 0.22. Single crystal X-ray diffraction analyses gave insight into their molecular structures and the packing arrangement. Evaluation of aromaticity in these multihelicenes revealed a non-aromatic character of the 2*H*-1,2-azaborole constituent rings.

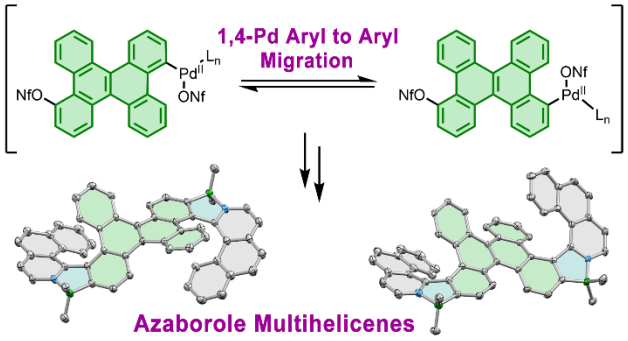

INTRODUCTION

Molecules embedding more than one (hetero)helicene[1] unit are referred to as multiple (hetero)helicenes or multi(hetero)helicenes.[2-6] To date, a plethora of these fascinating molecules have been reported, including double, triple, quadruple, quintuple and even sextuple analogues.[7-15] Interest in these compounds evolved naturally from research on planar and contorted polycyclic aromatic

hydrocarbons (PAHs).[16-18] The incorporation of helical moieties into π-conjugated structures adds a new dimension to their functionality, enabling the realization of new-generation devices, such as circularly polarized organic-light emitting diodes, polarization-selective photodetectors, and spintronic devices.[19-22] To improve their performance, a large variety of chiral materials have been developed and studied, contributing to a better understanding and control of their chiroptical properties, the orientation of the molecules relative to other device components, and the packing arrangement.[23-26] Dibenzo[*g*,*p*]chrysene (**DBzC**) with its inherently twisted structure constitutes a unique representative of contorted PAHs,[27] and an appealing candidate as a building block for the synthesis of various single and multiple helicene frameworks.[28-31] Over the past decade, several beautiful **DBzC** multihelicenes have been reported,[32-34] with only a few examples of multiheterohelicenes.[33, 35] Doping of PAHs with heteroatoms is an effective method for fine-tuning their optoelectronic properties.[36-37] For instance, the introduction of boron or a B-N motif leads to increased electron affinity, and improved photophysical properties.[38-55] However, the incorporation of heteroatoms into π-extended systems often requires functionalization of the all-carbon cores at positions that are difficult to access by conventional methods, which hinders the synthesis of these structures.

Notably, 1,n-Pd migrations coupled with subsequent reactions are powerful tools to generate synthetically challenging targets. To date, diverse Pd migration processes have been developed,[56-64] but surprisingly, a relatively little attention was given to the aryl to aryl migration. Since the seminal works of Larock[65] and Gallagher,[66] this type of migration has been observed in a narrow range of molecular scaffolds, i.e. conformationally labile biaryl substrates, which facilitate the incorporation of a voluminous metal atom.[67-69] The only example of employing a fused system in this process was the synthesis of a Pd complex of dibenz[*a*,*c*]anthracene with a stoichiometric amount of $Pd(PEt_3)_4$, where the Pd 1,4-shift at 160 °C was rather sluggish (10 days) and the desired complex was accompanied by several other products.[70] Except for this work, the 1,4-palladium migration has not been reported for rigid systems.

Herein, we describe a controllable through-space 1,4-Pd aryl to aryl migration on the **DBzC** platform, which allowed the synthesis of configurationally stable regioisomeric quadruple helicenes containing two azaborole units via a single synthetic route. This is the first example of a 1,4-Pd migration occurring on condensed PAH systems, where the generated Pd species is trapped by another reaction. We also show that this process can be turned off, providing access to the target molecules in a regioselective manner. The properties of these multihelicenes were studied by absorption and emission spectroscopy in solution and in the solid state, cyclic voltammetry and pulse techniques. We also provide insights into their chiroptical properties, configurational stability, molecular structures and packing arrangement. Finally, the aromatic character of the target compounds has been evaluated based on magnetic and electronic criteria, addressing this intriguing aspect of azaborole chemistry.

RESULTS AND DISCUSSION

Synthesis and Optimization Studies

The synthesis of multihelicenes **MH1** and **MH2** requires stitching two benzoiso[*h*]quinoline (**BIQ**)[71] moieties onto the **DBzC** core at 1,9- and 1,8-positions, respectively. The key **DBzC** building blocks, functionalized in the bay areas, are challenging to be obtained by traditional methods. To date, only a few bay-dibrominated examples have been reported.[72-73] They are however incompatible in cross-coupling reactions with sterically encumbered α-pyridine derivatives, which are usually ineffective in Suzuki coupling,[74] while their metallated derivatives are inaccessible. Therefore, the reaction of choice was the Suzuki coupling between the chlorinated *N*-heterocycle and the borylated **DBzC** partners. Their precursors were 1,9- and 1,8-substituted nonaflates **DBzC-1,9-ONf** and **DBzC-1,8-ONf** (Schemes S1 and S2, Supporting Information), as the ONf group proved to be the most effective leaving group in the synthesis of other azaborole helicenes.[71, 75-78] Conversion of these compounds to the Bpin analogs by Pd-catalyzed Miyaura borylation with B_2pin_2 was performed under standard conditions using

potassium acetate and Pd(dppf)Cl_2 in dry and degassed *N*,*N*-dimethylformamide under argon atmosphere. To our surprise, regardless of the precursor used, each reaction produced a mixture of **DBzC-1,8-Bpin** and **DBzC-1,9-Bpin** in combined yields of 0-54 % (Scheme 1a). ^{1}H NMR revealed two sets of signals with essentially equal intensity. Thus, the regioisomers were formed in a 50:50 ratio (Figure 1a), indicating a thermodynamic control in their formation. Two distinct well-separated doublets of doublets at 8.75 and 8.58 ppm were assigned to the aromatic signals of **DBzC-1,9-Bpin**, while those at 8.68 and 8.64 ppm to the second isomer.

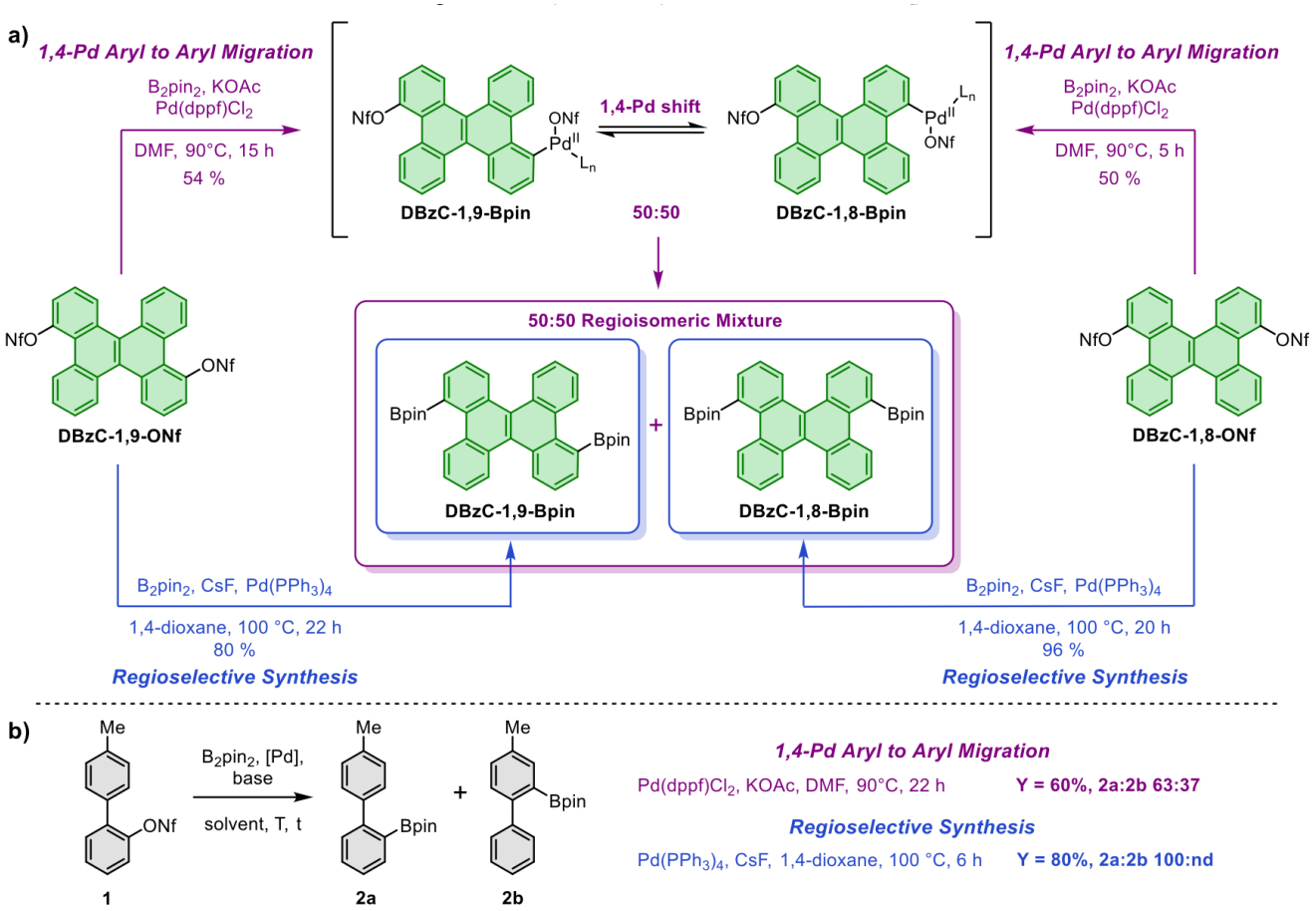

Scheme 1. Controllable 1,4-Palladium Migration/Miyaura Borylation for Model Compound **1** and **DBzC** Derivatives.

In addition, the spectrum shows two singlets at ca. 1.50 ppm corresponding to the non-equivalent Bpin methyl groups. We reasoned that this unexpected outcome can be attributed to a thermodynamically controlled 1,4-Pd migration in the bay region of the **DBzC** derivatives. However, it should be noted that the **DBzC-1,9-ONf** and **DBzC-1,8-ONf** can in principle undergo two-fold 1,4-Pd migration, leading to the compounds with substitution patterns equivalent to those of the starting materials due to the molecular symmetry. That means that only one-fold Pd-migration gives rise to the regioisomeric mixture. This process, most likely promoted by the acetate base, involves the oxidative addition of the organic nonaflate to Pd(0) and the remote C-H activation of the other bay position, leading to the formation of the regioisomeric products. Our synthesis of Bpin-substituted **DBzC** is the first practical demonstration of using Pd 1,4-migration in fused systems to prepare complex PAHs, where the generated Pd species is trapped with the diboron reagent in the Miyaura borylation. This tandem reaction has not been studied so far not only for fused systems, but also for flexible biaryls.
Due to the lack of sufficient separation of the resulting Bpin regioisomers by conventional purification methods, the first approach to **MH1** and **MH2** was the conversion of the regioisomeric mixture into

DBzC-1,8-BIQ and **DBzC-1,9-BIQ** (Scheme S3). The Suzuki-Miyaura cross-coupling of **DBzC-1,8-Bpin** and **DBzC-1,9-Bpin** with **BIQ-Cl** afforded the target compounds in a 59 % yield, also as a 1:1 regioisomeric mixture. Their further purification was extremely difficult due to the presence of several atropisomers, i.e. the corresponding (R_a,R_a) and (S_a,S_a)-enantiomers and the *meso*-compounds with similar or nearly identical retention times. Therefore, the mixture of teraryls was directly submitted to the electrophilic borylation with BBr_3 in the presence of Hünig's base to form the helical scaffolds, followed by a ligand exchange on boron with $AlMe_3$. Surprisingly, the reaction control via TLC indicated the formation of only two products. The compounds isolated by standard column chromatography and subsequent preparative TLC in a total yield of 38% were identified as the racemic mixture of multihelicenes **MH1** and **MH2**.[79] Thus, the 1,4-Pd migration process can be utilized to access the desired helicenes from the same starting material, reducing the synthetic effort.

The multihelicenes **MH1** and **MH2** embed two azabora[7]helicenes with high resistance to helical inversion at room temperature and two fluxional carbo[4]helicene moieties, resulting in up to six possible conformations in each case (see Computations section in the Supporting Information, the nomenclature used for the *M* and *P* stereodescriptors starts with the left azabora[7]helicene and continues counter-clockwise).

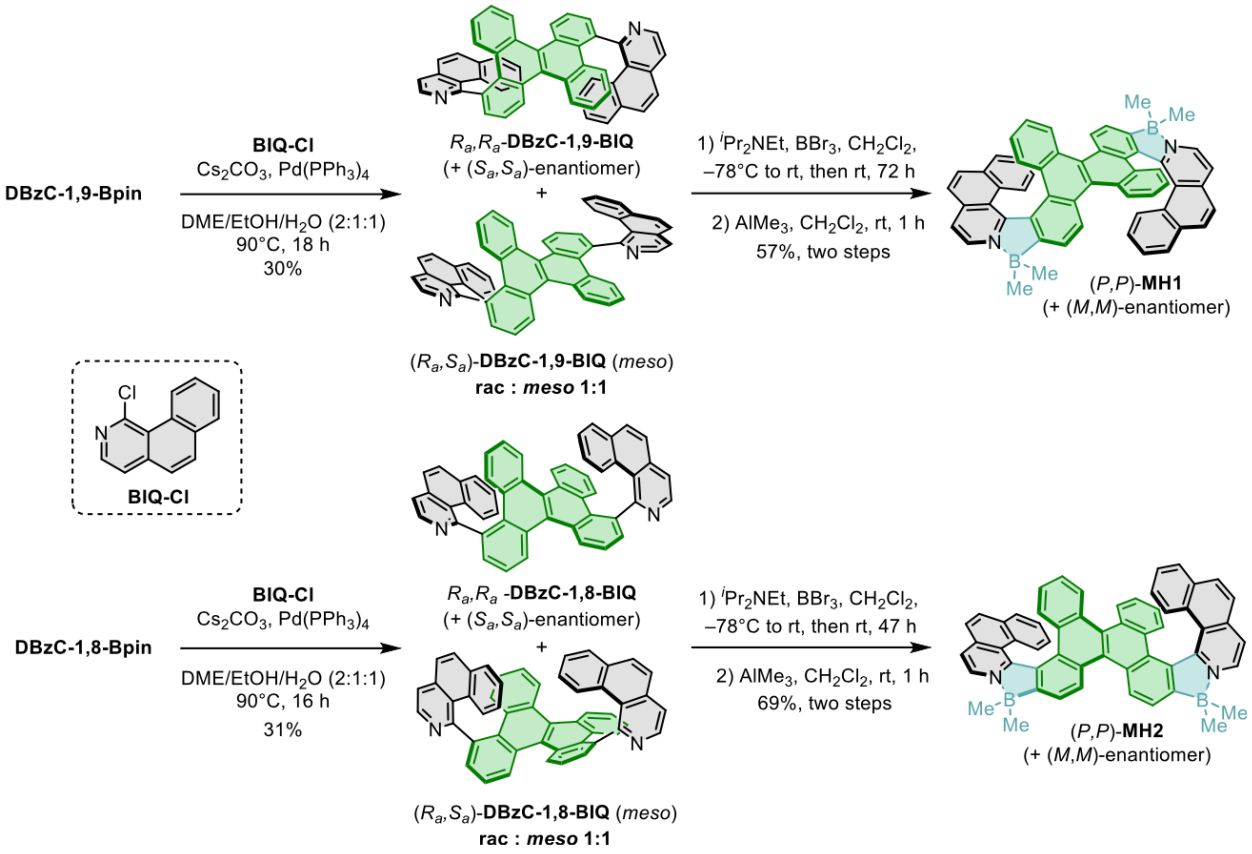

Scheme 2. Synthesis of Target Multihelicenes **MH1** and **MH2** from Regioisomerically Pure Precursors.

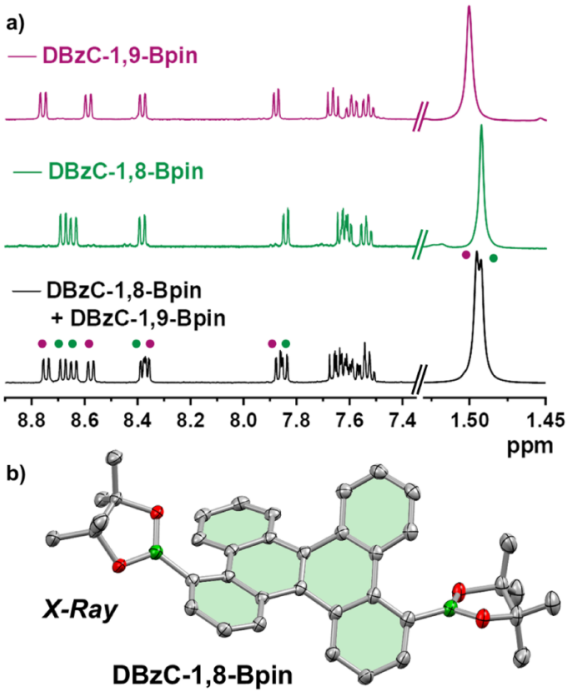

Figure 1. a) ^{1}H NMR spectra of the regioisomeric mixture of **DBzC-1,9-Bpin** and **DBzC-1,8-Bpin** and the isolated regioisomers in CD_2Cl_2 at 298 K. b) Molecular structure of **DBzC-1,8-Bpin** determined by X-ray diffraction analysis at 100 K (CCDC 2353062). Thermal ellipsoids are shown with 50% probability. Hydrogen atoms were omitted for clarity.

As indicated by DFT calculations (ωB97XD[80]/def2-TZVP[81-82]//ωB97XD/def2-SVP[81-82]), the most stable diastereomer of **MH1**, (*PMPM*)-**C1-MH1**, possesses azabora[7]- and carbo[4]helicene moieties of opposite helicities. This result is consistent with the single crystal X-ray analysis (*vide infra*) of **MH1** (Figure 2), showing the thermodynamically most stable conformation. Likewise, the (*PMPM*)-**C1-MH2** is the thermodynamically preferred diastereomer. However, it is only slightly lower in energy (by 1.7 kJ mol^{-1} in the gas phase) than (*PPPM*)-**C4-MH2**, observed in the solid state (Figure 2). The absence of **MH1** and **MH2** with mixed *P* and *M* helicities of the azaborahelicene moieties in a single molecule can be rationalized by their higher relative energies. Due to the presence of as many as four helical moieties, the enantiomerization mechanisms of both **MH1** and **MH2** are complex, with the preferred pathways computationally characterized by $\Delta G_{enant}^{\ddagger}$ of ca. 149 kJ·mol^{-1} for the rate-determining steps (gas phase at 298 K, see Figures S94 and S95). Experimentally, the configurational stability of **MH1** and **MH2** was studied by thermal racemization at 170 °C in *ortho*-dichlorobenzene or at 190 °C in 1,2,4-trichlorobenzene, following the decay of the enantiomeric excess either by electronic circular dichroism (ECD) or by analytical chiral HPLC to provide $\Delta G_{enant}^{\ddagger}$ of 141 and 143 kJ·mol^{-1}, respectively (see Figures S87 and S88).
The intrinsic limitation of the non-regioselective synthesis, i.e. the overall low yield of each regioisomer, as the key ONf intermediate is evenly distributed between the two synthetic pathways, and the challenging purification, prompted us to develop a regioselective synthesis of **MH1** and **MH2**. The key to achieving this goal is suppressing the 1,4-Pd migration process during the Miyaura borylation of **DBzC-1,8-ONf** and **DBzC-1,9-ONf**. To identify the suitable reaction conditions, we studied this transformation on the readily accessible unsymmetrical biphenyl prototype **1** bearing a nonaflate functionality at the *ortho* position (Scheme 1b and Table S1). When **1** was allowed to react with B_2pin_2 under the conditions we applied for the synthesis of **DBzC-1,8-Bpin** and its 1,9 regioisomer, both the direct borylation product **2a** and the migration/borylation product **2b** were formed in a 63:37 ratio

(Scheme 1b and Table S1, entry 1). This suggest that, under comparable reaction conditions, the 1,4-Pd migration is faster in the rigid palladium complexes derived from **DBzC-1,8-ONf** and its 1,9 regioisomer than in the flexible palladium complex derived from **1**. Already the change of the catalyst from $Pd(dppf)Cl_2$ to $Pd(PPh_3)_4$ resulted in a significant shift toward the retention product **2a** (87:13, entry 2). Afterwards, the impact of the solvent and the base was investigated. Replacing potassium acetate with KF, CsF and K_3PO_4 (entries 6 and 7) yielded **2a** as the exclusive product. These results support the hypothesis of the critical role of acetate in promoting the 1,4-Pd shift. To gain further insight into this process, we have carried out DFT calculations for the ONf-substituted biphenyl under the conditions described in entries 4 and 5 (Table S1). The most plausible mechanism appears to involve a reversible acetate-mediated deprotonation of the remote bay position, the formation of the five-membered palladacycle, and the subsequent protonation, which results in net 1,4-Pd migration (see Scheme S5, Figure S96 and the discussion in the Supporting Information).

Ultimately, the optimized catalytic system consisting of B_2pin_2, CsF and $Pd(PPh_3)_4$ in 1,4-dioxane at 110°C provided exclusively **2a** in 80 % yield, with no detectable amount of **2b** (Scheme 1b and Table S1, entry 7). Under these conditions, the 1,4-Pd migration process is totally suppressed for prototype **1**. Noteworthy, we did not manage to significantly shift the outcome of the model reaction to the migration product (Table S1, entries 9–12).

The optimized conditions were then transferred to the borylation of **DBzC-1,8-ONf** and **DBzC-1,9-ONf** with B_2pin_2. To our delight, **DBzC-1,8-Bpin** and **DBzC-1,9-Bpin** were isolated in 96% and 80% yields, respectively, with no migration products observed (Scheme 1a). The molecular structure of **DBzC-1,8-Bpin** was unambiguously confirmed by solid state structural analysis (Figure 1b).

With pure **DBzC-1,8-Bpin** and **DBzC-1,9-Bpin** in hand, we proceeded with the synthesis of multihelicenes, following the same synthetic route, as described above for the regioisomeric mixture (Scheme 2). Accordingly, two-fold Suzuki-Miyaura cross-coupling of the Bpin-substituted compounds with **BIQ-Cl** selectively furnished teraryls **DBzC-1,8-BIQ** and its 1,9 regioisomer in 31 and 30% yields, respectively. In both cases, the ^{1}H NMR spectra of the isolated products revealed two sets of signals with a 1:1 ratio, which we have assigned to a mixture of the racemates and the *meso*-compounds. This assumption was confirmed by analytical HPLC on a chiral stationary phase. The chromatograms of both products showed clearly visible three peaks (Figure S82). Their deconvolution and integration provided the ratios of 2:1:1 and 1:2:1 for **DBzC-1,9-Bpin** and **DBzC-1,8-Bpin**, respectively, which are attributed to the (S_a,S_a)-, (R_a,R_a)-, and (R_a,S_a)-diastereomers (Figure S85). The conversion of these diastereomeric mixtures to the target multihelicenes was efficient, selectively yielding **MH1** and **MH2** in 57% and 69% yields, respectively, over two steps.

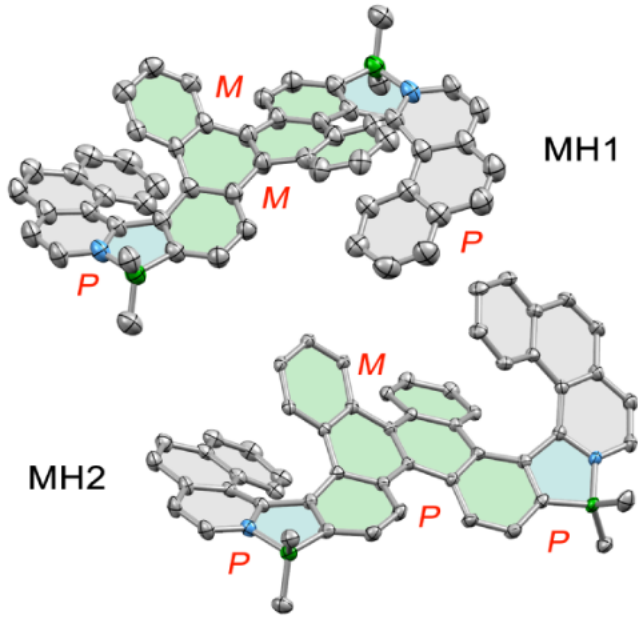

Figure 2. Molecular structures of **MH1** (CCDC 2353061) and **MH2** (CCDC 2353060) determined by X-ray analysis at 100 K. Thermal ellipsoids are shown with 50% probability. Hydrogen atoms were omitted for clarity.

Optical Properties

To elucidate the effect of the presence of two azabora[7]helicene moieties and their mutual arrangement on the photophysical properties of the multihelicenes, their absorption and emission spectra were measured in solution and in the solid state. The results are summarized in Table 1. Both regioisomers show intense yellow color in dichloromethane (Figure 3b) and yellow-orange color in the solid state. These observations are in good agreement with the recorded absorption spectra (Figure 3a). The lowest-energy absorption bands in dichloromethane solutions are located at 460 nm and 461 nm for **MH1** and **MH2**, respectively. Moreover, a slightly hypsochromically shifted shoulders (vibronic progressions) are observed for both compounds at 445 nm (**MH1**) and 443 nm (**MH2**). The corresponding molar extinction coefficients (ε) are moderate, in the range of 4.6–8.6 × 10^3 M^{-1} cm^{-1}. According to DFT calculations (ωB97XD/def2-SVP, solvent CH_2Cl_2), these absorption bands are superpositions of several transitions (Figures S98 and S101, Tables S9-S11, Supporting Information). In contrast to **MH1**, its regioisomer **MH2** exists as a mixture of two relevant conformers **C1-MH2** and **C4-MH2**, differing in the configuration of the labile carbo[4]helicene moiety, with the relative population of 79 and 21% in dichloromethane at 298 K. The first, most intensive transitions in the spectra of these two species and of **MH1** (oscillator strengths (f) of 0.46-0.51) are predominantly attributed to the HOMO ⟶ LUMO transitions (59-64%). In general, the LUMOs are uniformly delocalized over the whole molecules, while the HOMOs have larger coefficients on the **DBzC** central core (Figure S97, Supporting Information).

The bright green fluorescence of dichloromethane solutions of **MH1** and **MH2** (Figure 3b) coincides with the emission maxima at 527 nm and 523 nm for **MH1** and **MH2**, resulting in the large apparent Stokes shifts of 2760 cm^{-1} and 2570 cm^{-1}, respectively. The emission quantum yields of 0.26 (**MH1**) and 0.29 (**MH2**) are relatively high for helicenes built from *ortho*-fused rings and the fluorescence lifetimes (τ_{fl}) reach the averaged values of 7.1 ns (**MH1**) and 6.7 ns (**MH2**).

In the solid state, the regioisomers differ in their absorption behavior. **MH1** shows a blue-shift of its first absorption maximum, while the band of **MH2** is bathochromically shifted, which indicates different packing arrangements of these regioisomers. This assumption is further reinforced by the shifts of the emission bands, following the same trend as observed for the solid-state absorption

spectra (Figure 3b). Accordingly, the maxima are centered at 523 nm (**MH1**) and 553 nm (**MH2**) and correspond to green or green-yellow emission color. The bathochromic shift in the case of **MH2** is pronounced (1040 cm^{-1}) compared to the small hypsochromic shift for **MH1** (150 cm^{-1}). The Φ values in the solid state for both **MH1** and **MH2** are lower than the corresponding values measured in solution (0.16 and 0.22, respectively).
Compared with the recently reported single azabora[7]helicene **EH3**[75] built on a **DBzC** core, the additional helical units in **MH1** and **MH2** result in a bathochromic shift of both absorption (1040-1090 cm^{-1}) and emission maxima (490-630 cm−1) in solution, while the Φ_{fl} values in dichloromethane are comparable. Thus, the introduction of an additional azaborole helicene allows the modulation of the optical response toward higher wavelengths, while maintaining the emission efficiency in solution. On the other hand, the emission of **MH2** in the solid state is significantly higher than that of **EH3** (Φ_{PL} = 0.13).[75]

Single Crystal X-Ray Diffraction Analysis
To get insight into the molecular structures and the packing arrangements of the target multihelicenes and their intermediates, we grew crystals of **DBzC-1,8-Bpin** (for the packing arrangement, see the Supporting Information), rac-**MH1** and rac-**MH2** by diffusion of *n*-hexane into their dichloromethane solutions. The compounds crystallized in the space groups $P\bar{1}$, $P2_1/c$**,** and $P2_1/n$, respectively. The analysis of **MH2** (Figure 2) showed B-N bond lengths of 1.618(1) and 1.622(2) Å, indicating strong Lewis pair interactions and stable azaborole rings. It also revealed the (*PPPM*)-conformer (and enantiomeric (*MMMP*)-conformer), referred to as **C4-MH2**, which was identified by DFT calculations to be slightly higher in energy than the thermodynamically preferred (*PMPM*)-conformer **C1-MH2** in the gas phase (*vide supra*). Along the long molecular edge, the neighboring homochiral molecules are interchangeably rotated by 90° (Figure S80a,b, Supporting Information), resulting in pronounced face-to-edge C–H···π interactions between the homochiral molecules (Figure S80d). In contrast, the interactions between the heterochiral molecules with a significant offset are less distinctive (Figure S80c). These include only C–H···π interactions, and no π-π interactions. Apparently, the highly twisted structure of the multihelicene in combination with the inherent distortion of the **DBzC** core effectively reduces the π-π interactions, which is also reflected in the high solubility of **MH2**.
Numerous attempts to grow single crystals of **MH1** suitable for an X-ray diffraction analysis provided crystals showing complete molecular disorder over the inversion center, and despite our efforts, it was not possible to obtain direct evidence on the packing arrangement of **MH1**. However, the analysis unambiguously revealed the (*PMPM*)-conformer **C1-MH1** (Figure 2).

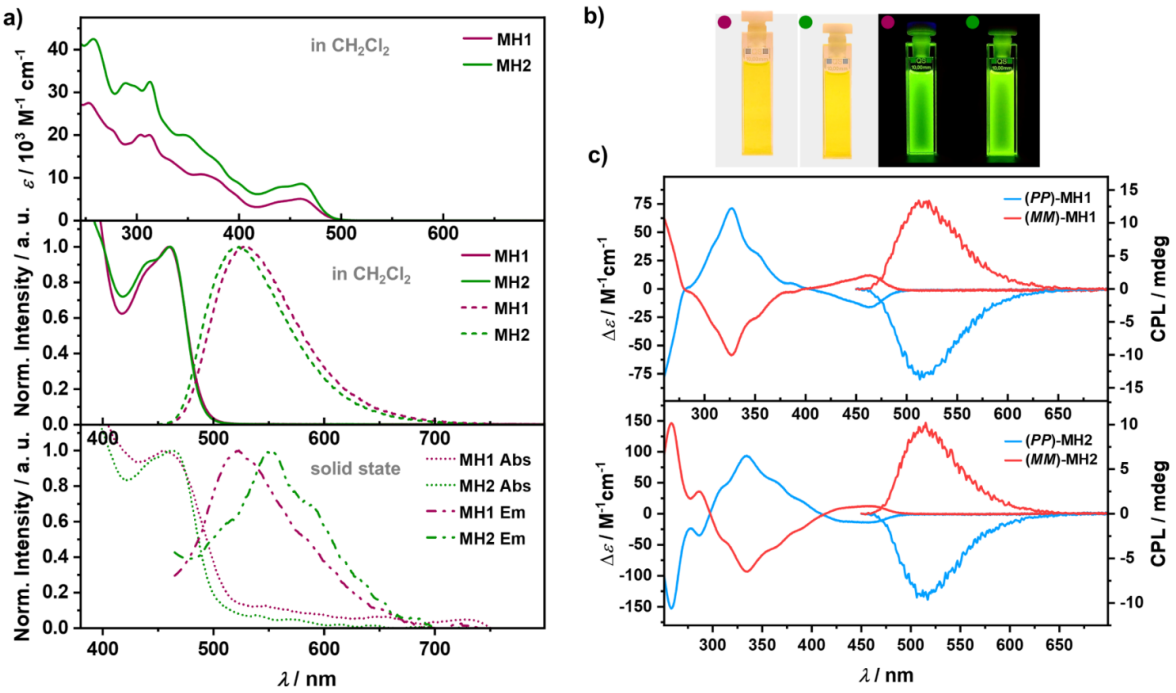

Figure 3. a) Top: Absorption spectra of **MH1** and **MH2** in CH_2Cl_2 solutions (**MH1**: c = 5.7 ×10^{-5} M, **MH2**: c = 5.4 ×10^{-5} M). Middle: Normalized absorption and emission spectra in CH_2Cl_2 solutions (**MH1**: c = 2.0 × 10^{-5} M, **MH2**: c = 1.2 × 10^{-5} M, λ_{ex} = 440 nm). Bottom: Normalized absorption (thin films obtained from CH_2Cl_2 solutions on quartz glass) and emission (amorphous powder) spectra in the solid state. b) Photographs of CH_2Cl_2 solutions of **MH1** and **MH2** under visible light and UV light c) ECD (**MH1**: c = 3.8 × 10^{-5} M, **MH2**: 2.6 × 10^{-5} M) and CPL (**MH1**: c = 9.0 × 10^{-6} M; **MH2**: 9.2 × 10^{-5} M) spectra in CH_2Cl_2.

Table 1. Optical Properties of **MH1** and **MH2**.

Cpd.	λ_{abs}[a] / nm	ε_{max}[b] / 10^3 M^{-1} cm^{-1}	λ_{em}[c] / nm	Stokes shift / cm^{-1}	Φ_{fl}[d]	τ_1[e] / ns (% amp)	τ_2[e] / ns (% amp)	τ[f] / ns	λ_{abs}[g] / nm	λ_{em}[h] / nm	Φ_{PL}[i]
MH1	460 445	5.1 4.6	527	2760	0.26	2.8 (0.046)	7.3 (95.4)	7.1	454	523	0.16
MH2	461 443	8.6 7.9	523	2570	0.29	2.3 (0.049)	6.9 (95.1)	6.7	464	553	0.22

[a] Absorption maximum in CH_2Cl_2. [b] Molar absorption coefficient. [c] Fluorescence maximum in CH_2Cl_2. [d] Absolute fluorescence quantum yield in CH_2Cl_2. [e] Fluorescence lifetime (relative % amplitude). [f] Amplitude-weighted average fluorescence lifetime. [g] Absorption maximum in the solid state. [h] Emission maximum in the solid state. [i] Photoluminescence quantum yield in the solid state.

Table 2. Chiroptical Properties of **MH1** and **MH2**.

Cpd.	$\lvert g_{abs}\rvert$[a] / 10^{-3}	$\lvert g_{lum}\rvert$[b] / 10^{-3}	B_{CPL}[c] M^{-1} cm^{-1}
MH1	4.9 (328 nm), 1.7 (460 nm)	2.7 (512 nm)	1.79
MH2	4.6 (335 nm), 1.9 (460 nm)	2.2 (515 nm)	2.75

[a] Absorption dissymmetry factor at a given wavelength in parentheses. [b] Luminescence dissymmetry factor at a given wavelength in parentheses. [c] CPL brightness calculated as $B_{CPL} = \varepsilon \times \Phi \times \lvert g_{lum}\rvert/2$.

Chiroptical Properties

To investigate the chiroptical properties of the multihelicenes, the racemic mixtures of **MH1** and **MH2** were resolved via semi-preparative HPLC on a chiral stationary phase (for details, see the Supporting Information). By comparing the experimental electronic circular dichroism (ECD) spectra with the simulated spectra (TD-DFT calculations, Figures S98, S100, S101, and S103), the first isolated fraction was assigned to the (*PP*)-enantiomer, while the second fraction to the (*MM*)-enantiomer (note: only the descriptors for the two configurationally stable azabora[7]helicene fragments are used). Their ECD and circularly polarized luminescence (CPL) spectra were recorded in dichloromethane (Figure 3c and Table 2). The ECD of (*PP*)-**MH1** shows a negative Cotton effect at 463 nm ($\Delta\varepsilon$ = –16 M^{-1} cm^{-1}) and a positive Cotton effect at 328 nm ($\Delta\varepsilon$ = 71 M^{-1} cm^{-1}). (*PP*)-**MH2** reveals a similar line shape with a negative Cotton effect at 458 nm ($\Delta\varepsilon$ = –14 M^{-1} cm^{-1}) and a positive Cotton effect at 334 nm ($\Delta\varepsilon$ = 94 M^{-1} cm^{-1}). The enantiomers manifest a mirror image relationship, and the dissymmetry factors $|g_{abs}|$ reach the highest values of 4.9×10^{-3} at 328 nm for **MH1** and 4.6×10^{-3} at 335 nm for **MH2**. The $|g_{abs}|$ corresponding to the lowest-energy bands are smaller, i.e. 1.7×10^{-3} and 1.9×10^{-3}, respectively. The compounds also show CPL activity. Like the CD spectra, the CPL spectra of their (*MM*)- and (*PP*)-enantiomers unfold mirror image relationship, with the maxima for (*MM*)-**MH1** and (*MM*)-**MH2** positioned at 515 nm and 513 nm, respectively. These positive bands correspond to the $|g_{lum}|$ factors of 2.7×10^{-3} for **MH1** and 2.2×10^{-3} for **MH2**.

CPL brightness (B_{CPL}) of **MH1** and **MH2**, defined as $B_{CPL} = \varepsilon \times \Phi \times |g_{lum}|/2$, combines the absorption coefficient, the emission quantum yield in solution, and the dissymmetry factor efficiencies to give a more accurate evaluation of the overall efficiency of a chiral emitter.[75] The values for **MH1** and **MH2** of 1.79 M^{-1} cm^{-1} and 2.75 M^{-1} cm^{-1}, respectively, are within the typical range for most of the azaborole helicenes.

Electrochemistry

The electrochemical properties of **MH1** and **MH2** were investigated by cyclic voltammetry (CV) and square wave voltammetry (SW) in dichloromethane in the presence of *n*-Bu_4NPF_6 as a supporting electrolyte and calibrated against ferrocenium/ferrocene (Fc^+/Fc). The redox potentials are summarized in Table S8 and the voltammograms are depicted in Figure S93 (Supporting Information). Both compounds undergo one irreversible reduction and three oxidation processes. The oxidation potentials of **MH1** are located at +0.56, +0.72 and +1.03 V (SW) and are comparable to those of **MH2** (ca. +0.62, +0.74 and ca. 1.03, SW). The reduction of **MH1** and **MH2** occurs at –2.24 V (SW) and –2.22 V (SW), respectively. This differs from the behavior of single azabora[7]helicene **EH3**, for which two oxidation and two reduction events can be observed. The addition of a second azaborole [7]helicene fragment to the **DBzC** core results in a slight cathodic shift of both E^{ox1} and E^{red1} by 0.10-0.16, leading to the elevation of the HOMO and LUMO energy levels for both compounds compared to **EH3**.[75]

Aromaticity

An intriguing question is the aromaticity of azaboroles and PAHs that incorporate this heterocycle. While the aromatic character of simple five-membered boracycles containing several heteroatoms (B, N, O, S) has been studied,[83-84] this aspect remained unresolved for 2*H*-1,2-azaborole, a constituent heterole of our helicenes. To address this question, we examined aromaticity in multihelicenes **MH1** and **MH2** using 3D isocontours maps of isotropic magnetic shielding (IMS)[85] and the electron density of delocalized bonds (EDDB).[86] These analyses revealed that both **MH1** and **MH2** are aromatic molecules: the 3D IMS isocontours maps (Figure 4a) show only positive values of IMS (visualized by the blue color and attributed to aromaticity) over the six-membered rings, and the fraction of delocalized electrons is ca. 76.1–77.2% according to the $EDDB_H(r)$ analyses (Figure 4b). The non-equivalent magnetic and electronic environment of both sides of each ring, inherent to the chirality of **MH1** and **MH2**, is clearly visualized in these analyses. Expectedly, the values of IMS over the azaborole rings are of small

magnitude (|IMS| < 5.5 ppm, visualized by the neutral color) indicating a non-aromatic character of these rings, as opposed to the structurally related antiaromatic boroles.[87-88] The non-aromaticity of azaboroles was confirmed by the EDDB isovalue plots showing no electron density over the B–N and B–C bonds. Thus, the Clar structures[89-90] of **MH1** and **MH2** contain eight π-sextets and three isolated double bonds (Figure 4c).

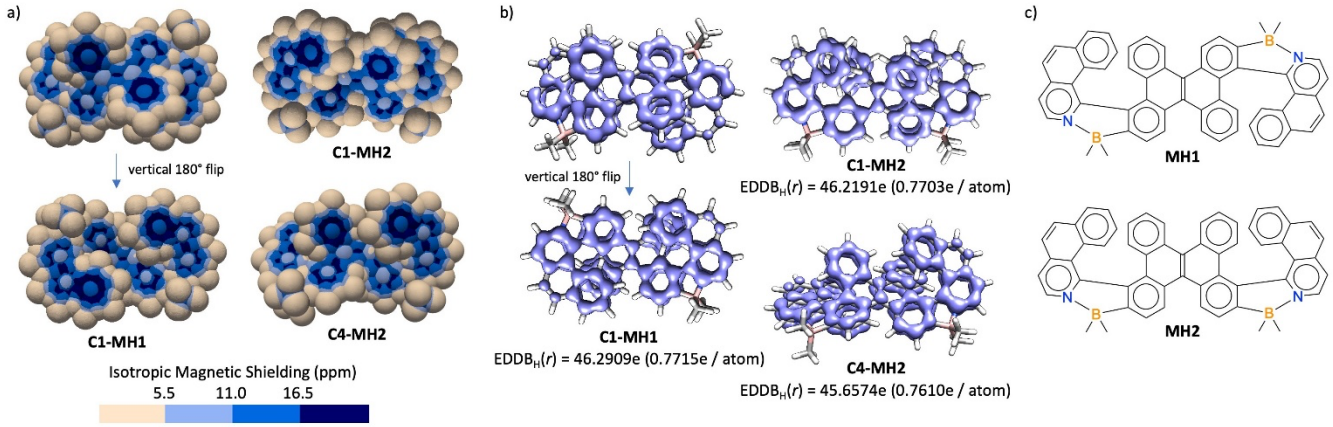

Figure 4. a) 3D isocontours maps of isotropic magnetic shielding (IMS) of **C1-MH1**, **C1-MH2** and **C4-MH2**. b) Plots of the electron density of delocalized bonds [EDDB$_H$(r)] of **C1-MH1**, **C1-MH2** and **C4-MH2**; isovalue = 0.025. c) The Clar structures of **MH1** and **MH2**.

CONCLUSIONS

We have developed the synthesis of two original regioisomeric quadruple helicenes **MH1** and **MH2** embedding two azaborole [7]helicene units, the first configurationally stable azaborole multihelicenes. The key step of the synthetic sequence was the borylation of 1,9- and 1,8-nonaflate-substituted **DBzC** derivatives. Their reactions with B_2pin_2 under conditions that are well-known to facilitate the C-H activation induced the 1,4-Pd aryl to aryl migration, leading to the formation of equal amounts of both regioisomers and in turn, allowed the synthesis of the target helicenes from the same starting material. To our knowledge, this is the first example of a tandem reaction on fused systems involving a 1,4-Pd shift.

Importantly, the outcome of this reaction can be controlled by the choice of the base and the catalytic system. Our experiments demonstrated the central role of the acetate, presumed to act as a proton shuttle, in promoting the through-space activation of the C-H bond at a remote bay position of **DBzC**. The reactions employing $Pd(PPh_3)_4$ as catalyst in absence of acetate bases enabled the controlled C-B bond formation at the positions originally occupied by the nonaflate groups, giving access to the regioisomerically pure azaborole multihelicenes **MH1** and **MH2** in excellent yields.

These compounds exhibit green fluorescence in dichloromethane with appreciable quantum yields of up to 0.29 and 0.22, respectively, and $|g_{lum}|$ of up to 2.7×10^{-3}. In the solid state, **MH1** and **MH2** show green or green-yellow emission with Φ_{PL} of up to 0.22 for the latter compound. While the spectra of **MH1** are hypsochromically shifted versus the spectra in solution, those of **MH2** show a pronounced bathochromic shift. Compared to a single azaborole helicene derived from **DBzC**,[75] the incorporation of a second helicene fragment proved particularly beneficial for the chiroptical responses of **MH1** and the emission intensity in the solid state of **MH2**, while shifting the spectra bathochromically. The presence of a second azaborole helicene fragment also altered the electrochemical response compared to monohelicene analog, albeit **MH1** and **MH2** have comparable electrochemical profiles. Thus, increasing the number of azaborole helicene fragments in combination with an extended π-system can serve as a viable strategy to gain access to materials whose properties may be further modulated by the mutual arrangement of helical fragments. In addition, using magnetic and electronic criteria, the

aromaticity patterns of **MH1** and **MH2** can be visualized and compared, which revealed the non-aromatic character of 2*H*-1,2-azaborole constituent rings.
Overall, these results enrich the structural diversity of dibenzochrysene PAHs while improving some of their properties. We also envision that the conditions of 1,4 palladium migration can be applied to other fused systems, allowing the synthesis of PAHs with substitution patterns that may be difficult to access otherwise. Efforts in this direction are underway in our laboratories.

ASSOCIATED CONTENT

Supporting Information. Synthetic procedures, characterization details, HPLC resolution, cyclic voltammetry and square wave voltammetry data, crystal structural data, racemization studies, photophysical and chiroptical studies, computational details. The 3D IMS isocontours maps are interactive and are available for visualization (and personalization) in the Supporting Information as .vtk files. This material is available free of charge via the Internet at http://pubs.acs.org.

AUTHOR INFORMATION

Corresponding Author

* **Agnieszka Nowak-Król** − Institut für Anorganische Chemie and Institute for Sustainable Chemistry & Catalysis with Boron, Julius-Maximilians-Universität Würzburg, 97074 Würzburg, Germany; orcid.org/0000-0003-0454-2491;
Email: agnieszka.nowak-krol@uni-wuerzburg.de.

Notes

The authors declare no competing financial interest

Accession Codes

CCDC 2353062 (**DBzC-1,8-Bpin**), 2353061 (**MH1**), and 2353060 (**MH2**) contain the supplementary crystallographic data for this paper. These data can be obtained free of charge *via* www.ccdc.cam.ac.uk/data_request/cif, or by emailing data_request@ccdc.cam.ac.uk, or by contacting The Cambridge Crystallographic Data Centre, 12 Union Road, Cambridge CB2 1EZ, UK; fax: +44 1223 336033.

ACKNOWLEDGMENT

A.N.-K. thanks the German Research Foundation (DFG) for an Emmy-Noether Fellowship (NO 1459/1-1). A.N.-K. and F.F. thank the Hector Fellow Academy (HFA) for financial support. A.A. acknowledges the European Union's Framework Programme for Research and Innovation Horizon Europe under the Marie Skłodowska-Curie Grant Agreement No. 101106492 (project title: Full-Fission). Y.C. thanks the French Agence Nationale de la Recherche—ANR for financial support (ANR-19-CE07-0041). The authors thank Dr. Krzysztof Radacki for providing a solution for the crystal structure of **MH1**, Prof. Todd B. Marder for use of his fluorimeter, and Dr. Yannick Carissan for the ims3d.py program.

REFERENCES

(1) For helically shaped tetracyclic *ortho*-fused polycyclic aromatic compounds, [4]helicene is an acceptable extension of the IUPAC definition of helicenes. Moss, G. P.; Smith, P. A. S.; Tavernier, D. Glossary of class names of organic compounds and reactivity intermediates based on structure (IUPAC Recommendations 1995). *Pure Appl. Chem.* **1995**, *67*, 1307-1375.
(2) Yang, W.-W.; Shen, J.-J. Multiple Heterohelicenes: Synthesis, Properties and Applications. *Chem. Eur. J.* **2022**, *28*, e202202069.
(3) Kato, K.; Segawa, Y.; Itami, K. Symmetric Multiple Carbohelicenes. *Synlett* **2019**, *30*, 370-377.

(4) Mori, T. Chiroptical Properties of Symmetric Double, Triple, and Multiple Helicenes. *Chem. Rev.* **2021**, *121*, 2373-2412.
(5) Wu, Y.-F.; Zhang, L.; Zhang, Q.; Xie, S.-Y.; Zheng, L.-S. Multiple [*n*]helicenes with various aromatic cores. *Org. Chem. Front.* **2022**, *9*, 4726-4743.
(6) Li, C.; Yang, Y.; Miao, Q. Recent Progress in Chemistry of Multiple Helicenes. *Chem. Asian J.* **2018**, *13*, 884-894.
(7) Tan, D.; Dong, J.; Ma, T.; Feng, Q.; Wang, S.; Yang, D.-T. Multiple Helicenes Defected by Heteroatoms and Heptagons with Narrow Emissions and Superior Photoluminescence Quantum Yields. *Angew. Chem. Int. Ed.* **2023**, *62*, e202304711.
(8) Katayama, T.; Nakatsuka, S.; Hirai, H.; Yasuda, N.; Kumar, J.; Kawai, T.; Hatakeyama, T. Two-Step Synthesis of Boron-Fused Double Helicenes. *J. Am. Chem. Soc.* **2016**, *138*, 5210-5213.
(9) Wang, X.-Y.; Wang, X.-C.; Narita, A.; Wagner, M.; Cao, X.-Y.; Feng, X.; Müllen, K. Synthesis, Structure, and Chiroptical Properties of a Double [7]Heterohelicene. *J. Am. Chem. Soc.* **2016**, *138*, 12783-12786.
(10) Aribot, F.; Merle, A.; Dechambenoit, P.; Bock, H.; Artigas, A.; Vanthuyne, N.; Carissan, Y.; Hagebaum-Reignier, D.; Coquerel, Y.; Durola, F. A Triply [5]Helicene-Bridged (1,3,5)Cyclophane. *Angew. Chem. Int. Ed.* **2023**, *62*, e202304058.
(11) Artigas, A.; Rigoulet, F.; Giorgi, M.; Hagebaum-Reignier, D.; Carissan, Y.; Coquerel, Y. Overcrowded Triply Fused Carbo[7]helicene. *J. Am. Chem. Soc.* **2023**, *145*, 15084-15087.
(12) Roy, M.; Berezhnaia, V.; Villa, M.; Vanthuyne, N.; Giorgi, M.; Naubron, J.-V.; Poyer, S.; Monnier, V.; Charles, L.; Carissan, Y.; Hagebaum-Reignier, D.; Rodriguez, J.; Gingras, M.; Coquerel, Y. Stereoselective Syntheses, Structures, and Properties of Extremely Distorted Chiral Nanographenes Embedding Hextuple Helicenes. *Angew. Chem. Int. Ed.* **2020**, *59*, 3264-3271.
(13) Berezhnaia, V.; Roy, M.; Vanthuyne, N.; Villa, M.; Naubron, J.-V.; Rodriguez, J.; Coquerel, Y.; Gingras, M. Chiral Nanographene Propeller Embedding Six Enantiomerically Stable [5]Helicene Units. *J. Am. Chem. Soc.* **2017**, *139*, 18508-18511.
(14) Hosokawa, T.; Takahashi, Y.; Matsushima, T.; Watanabe, S.; Kikkawa, S.; Azumaya, I.; Tsurusaki, A.; Kamikawa, K. Synthesis, Structures, and Properties of Hexapole Helicenes: Assembling Six [5]Helicene Substructures into Highly Twisted Aromatic Systems. *J. Am. Chem. Soc.* **2017**, *139*, 18512-18521.
(15) Zhang, F.; Michail, E.; Saal, F.; Krause, A.-M.; Ravat, P. Stereospecific Synthesis and Photophysical Properties of Propeller-Shaped C90H48 PAH. *Chem. Eur. J.* **2019**, *25*, 16241-16245.
(16) Baig, N.; Kammakakam, I.; Falath, W. Nanomaterials: a review of synthesis methods, properties, recent progress, and challenges. *Mater. Adv.* **2021**, *2*, 1821-1871.
(17) Li, Q.; Zhang, Y.; Xie, Z.; Zhen, Y.; Hu, W.; Dong, H. Polycyclic aromatic hydrocarbon-based organic semiconductors: ring-closing synthesis and optoelectronic properties. *J. Mater. Chem. C* **2022**, *10*, 2411-2430.
(18) Mingyu Sang; Jongwoon Shin; Kiho Kim; Yu, K. J. Electronic and Thermal Properties of Graphene and Recent Advances in Graphene Based Electronics Applications. *Nanomaterials* **2019**, *9*, 374.
(19) Brandt, J. R.; Salerno, F.; Fuchter, M. J. The added value of small-molecule chirality in technological applications. *Nat. Chem. Rev.* **2017**, *1*, 0045.
(20) Furlan, F.; Moreno-Naranjo, J. M.; Gasparini, N.; Feldmann, S.; Wade, J.; Fuchter, M. J. Chiral materials and mechanisms for circularly polarized light-emitting diodes. *Nat. Photonics* **2024**, *18*, 658-668.
(21) Ward, M. D.; Wade, J.; Shi, X.; Nelson, J.; Campbell, A. J.; Fuchter, M. J. Highly Selective High-Speed Circularly Polarized Photodiodes Based on π-Conjugated Polymers. *Advanced Optical Materials* **2022**, *10*, 2101044.
(22) Kiran, V.; Mathew, S. P.; Cohen, S. R.; Hernández Delgado, I.; Lacour, J.; Naaman, R. Helicenes—A New Class of Organic Spin Filter. *Adv. Mater.* **2016**, *28*, 1957-1962.

(23) Wade, J.; Salerno, F.; Kilbride, R. C.; Kim, D. K.; Schmidt, J. A.; Smith, J. A.; LeBlanc, L. M.; Wolpert, E. H.; Adeleke, A. A.; Johnson, E. R.; Nelson, J.; Mori, T.; Jelfs, K. E.; Heutz, S.; Fuchter, M. J. Controlling anisotropic properties by manipulating the orientation of chiral small molecules. *Nat. Chem.* **2022**, *14*, 1383-1389.
(24) Greenfield, J. L.; Wade, J.; Brandt, J. R.; Shi, X.; Penfold, T. J.; Fuchter, M. J. Pathways to increase the dissymmetry in the interaction of chiral light and chiral molecules. *Chem. Sci.* **2021**, *12*, 8589-8602.
(25) Crassous, J.; Fuchter, M. J.; Freedman, D. E.; Kotov, N. A.; Moon, J.; Beard, M. C.; Feldmann, S. Materials for chiral light control. *Nat. Rev. Mater.* **2023**, *8*, 365-371.
(26) Frédéric, L.; Desmarchelier, A.; Favereau, L.; Pieters, G. Designs and Applications of Circularly Polarized Thermally Activated Delayed Fluorescence Molecules. *Adv. Funct. Mater.* **2021**, *31*, 2010281.
(27) Hossain, M. M.; Mirzaei, M. S.; Lindeman, S. V.; Mirzaei, S.; Rathore, R. π-Extended dibenzo[g,p]chrysenes. *Org. Chem. Front.* **2021**, *8*, 2393-2401.
(28) Huang, H.-C.; Hsieh, Y.-C.; Lee, P.-L.; Lin, C.-C.; Ho, Y.-S.; Shao, W.-K.; Hsieh, C.-T.; Cheng, M.-J.; Wu, Y.-T. Highly Distorted Multiple Helicenes: Syntheses, Structural Analyses, and Properties. *J. Am. Chem. Soc.* **2023**, *145*, 10304-10313.
(29) Tsurusaki, A.; Kamikawa, K. Multiple Helicenes Featuring Synthetic Approaches and Molecular Structures. *Chem. Lett.* **2021**, *50*, 1913-1932.
(30) Li, C.; Yang, Y.; Miao, Q. Recent Progress in Chemistry of Multiple Helicenes. *Chem. Asian J.* **2018**, *13*, 884-894.
(31) Ren, M.; Wang, J.; Xie, X.; Zhang, J.; Wang, P. Double-Helicene-Based Hole-Transporter for Perovskite Solar Cells with 22% Efficiency and Operation Durability. *ACS Energy Lett.* **2019**, *4*, 2683-2688.
(32) Kashihara, H.; Asada, T.; Kamikawa, K. Synthesis of a Double Helicene by a Palladium-Catalyzed Cross-Coupling Reaction: Structure and Physical Properties. *Chem. Eur. J.* **2015**, *21*, 6523-6527.
(33) Fujikawa, T.; Mitoma, N.; Wakamiya, A.; Saeki, A.; Segawa, Y.; Itami, K. Synthesis, properties, and crystal structures of π-extended double [6]helicenes: contorted multi-dimensional stacking lattice. *Org. Biomol. Chem.* **2017**, *15*, 4697-4703.
(34) Ferreira, M.; Naulet, G.; Gallardo, H.; Dechambenoit, P.; Bock, H.; Durola, F. A Naphtho-Fused Double [7]Helicene from a Maleate-Bridged Chrysene Trimer. *Angew. Chem. Int. Ed.* **2017**, *56*, 3379-3382.
(35) Fujikawa, T.; Segawa, Y.; Itami, K. Synthesis and Structural Features of Quadruple Helicenes: Highly Distorted π Systems Enabled by Accumulation of Helical Repulsions. *J. Am. Chem. Soc.* **2016**, *138*, 3587-3595.
(36) Dhbaibi, K.; Favereau, L.; Crassous, J. Enantioenriched Helicenes and Helicenoids Containing Main-Group Elements (B, Si, N, P). *Chem. Rev.* **2019**, *119*, 8846-8953.
(37) Borissov, A.; Maurya, Y. K.; Moshniaha, L.; Wong, W.-S.; Żyła-Karwowska, M.; Stępień, M. Recent Advances in Heterocyclic Nanographenes and Other Polycyclic Heteroaromatic Compounds. *Chem. Rev.* **2022**, *122*, 565-788.
(38) von Grotthuss, E.; John, A.; Kaese, T.; Wagner, M. Doping Polycyclic Aromatics with Boron for Superior Performance in Materials Science and Catalysis. *Asian J. Org. Chem.* **2018**, *7*, 37-53.
(39) Nowak-Król, A.; Geppert, P. T.; Naveen, K. R. Boron-Containing Helicenes as New Generation of Chiral Materials: Opportunities and Challenges of Leaving the Flatland. *Chem. Sci.* **2024**, *15*, 7408-7440.
(40) Wakamiya, A.; Yamaguchi, S. Designs of Functional π-Electron Materials based on the Characteristic Features of Boron. *Bull. Chem. Soc. Jpn.* **2015**, *88*, 1357-1377.
(41) Farrell, J. M.; Grande, V.; Schmidt, D.; Würthner, F. A Highly Warped Heptagon-Containing sp2 Carbon Scaffold via Vinylnaphthyl π-Extension. *Angew. Chem. Int. Ed.* **2019**, *58*, 16504-16507.
(42) Neeve, E. C.; Geier, S. J.; Mkhalid, I. A. I.; Westcott, S. A.; Marder, T. B. Diboron(4) Compounds: From Structural Curiosity to Synthetic Workhorse. *Chem. Rev.* **2016**, *116*, 9091-9161.

(43) Radtke, J.; Schickedanz, K.; Bamberg, M.; Menduti, L.; Schollmeyer, D.; Bolte, M.; Lerner, H.-W.; Wagner, M. Selective Access to Either a Doubly Boron-Doped Tetrabenzopentacene or an Oxadiborepin from the Same Precursor. *Chem. Sci.* **2019**, *10*, 9017-9027.
(44) Vanga, M.; Lalancette, R. A.; Jäkle, F. Controlling the Optoelectronic Properties of Pyrene by Regioselective Lewis Base-Directed Electrophilic Aromatic Borylation. *Chem. Eur. J.* **2019**, *25*, 10133-10140.
(45) Narita, H.; Choi, H.; Ito, M.; Ando, N.; Ogi, S.; Yamaguchi, S. Fully Fused Boron-Doped Polycyclic Aromatic Hydrocarbons: Their Synthesis, Structure–Property Relationships, and Self-Assembly Behavior in Aqueous Media. *Chem. Sci.* **2022**, *13*, 1484-1491.
(46) Ito, M.; Sakai, M.; Ando, N.; Yamaguchi, S. Electron-Deficient Heteroacenes that Contain Two Boron Atoms: Near-Infrared Fluorescence Based on a Push–Pull Effect. *Angew. Chem. Int. Ed.* **2021**, *60*, 21853-21859.
(47) Su, X.; Bartholome, T. A.; Tidwell, J. R.; Pujol, A.; Yruegas, S.; Martinez, J. J.; Martin, C. D. 9-Borafluorenes: Synthesis, Properties, and Reactivity. *Chem. Rev.* **2021**, *121*, 4147-4192.
(48) Min, Y.; Dou, C.; Liu, D.; Dong, H.; Liu, J. Quadruply B←N-Fused Dibenzo-azaacene with High Electron Affinity and High Electron Mobility. *J. Am. Chem. Soc.* **2019**, *141*, 17015-17021.
(49) Hecht, R.; Kade, J.; Schmidt, D.; Nowak-Król, A. n-Channel Organic Semiconductors Derived from Air-Stable Four-Coordinate Boron Complexes of Substituted Thienylthiazoles. *Chem. Eur. J.* **2017**, *23*, 11620-11628.
(50) Ito, M.; Shirai, S.; Xie, Y.; Kushida, T.; Ando, N.; Soutome, H.; Fujimoto, K. J.; Yanai, T.; Tabata, K.; Miyata, Y.; Kita, H.; Yamaguchi, S. Fluorescent Organic π-Radicals Stabilized with Boron: Featuring a SOMO−LUMO Electronic Transition. *Angew. Chem. Int. Ed.* **2022**, *61*, e202201965.
(51) Zender, E.; Karger, S.; Neubaur, R.; Virovets, A.; Lerner, H.-W.; Wagner, M. Green-Emitting Extended B3,N2-Doped Polycyclic Aromatic Hydrocarbon with Multiple Resonance Structure. *Org. Lett.* **2024**, *26*, 939-944.
(52) Sano, Y.; Shintani, T.; Hayakawa, M.; Oda, S.; Kondo, M.; Matsushita, T.; Hatakeyama, T. One-Shot Construction of BN-Embedded Heptadecacene Framework Exhibiting Ultra-narrowband Green Thermally Activated Delayed Fluorescence. *J. Am. Chem. Soc.* **2023**, *145*, 11504-11511.
(53) Yuan, K.; Volland, D.; Kirschner, S.; Uzelac, M.; Nichol, G. S.; Nowak-Król, A.; Ingleson, M. J. Enhanced N-Directed Electrophilic C–H Borylation Generates BN–[5]- and [6]Helicenes with Improved Photophysical Properties. *Chem. Sci.* **2022**, *13*, 1136-1145.
(54) Appiarius, Y.; Míguez-Lago, S.; Puylaert, P.; Wolf, N.; Kumar, S.; Molkenthin, M.; Miguel, D.; Neudecker, T.; Juríček, M.; Campaña, A. G.; Staubitz, A. Boosting Quantum Yields and Circularly Polarized Luminescence of Penta- and Hexahelicenes by Doping with Two BN-Groups. *Chem. Sci.* **2024**, *15*, 466-476.
(55) Meng, G.; Zhou, J.; Han, X.-S.; Zhao, W.; Zhang, Y.; Li, M.; Chen, C.-F.; Zhang, D.; Duan, L. B-N Covalent Bond Embedded Double Hetero-[*n*]helicenes for Pure Red Narrowband Circularly Polarized Electroluminescence with High Efficiency and Stability. *Adv. Mater.* **2024**, *36*, 2307420.
(56) Shi, F.; Larock, R. C., Remote C–H Activation via Through-Space Palladium and Rhodium Migrations. In *C-H Activation*, Yu, J.-Q.; Shi, Z., Eds. Springer Berlin Heidelberg: Berlin, Heidelberg, 2010; pp 123-164.
(57) Dong, X.; Wang, H.; Liu, H.; Wang, F. Recent Advances in Transition Metal Migration Involving Reactions. *Org. Chem. Front.* **2020**, *7*, 3530-3556.
(58) Li, M.-Y.; Wei, D.; Feng, C.-G.; Lin, G.-Q. Tandem Reactions involving 1,4-Palladium Migrations. *Chem. Asian J.* **2022**, *17*, e202200456.
(59) Hu, T.-J.; Zhang, G.; Chen, Y.-H.; Feng, C.-G.; Lin, G.-Q. Borylation of Olefin C–H Bond via Aryl to Vinyl Palladium 1,4-Migration. *J. Am. Chem. Soc.* **2016**, *138*, 2897-2900.

(60) Huang, Q.; Fazio, A.; Dai, G.; Campo, M. A.; Larock, R. C. Pd-Catalyzed Alkyl to Aryl Migration and Cyclization: An Efficient Synthesis of Fused Polycycles via Multiple C–H Activation. *J. Am. Chem. Soc.* **2004**, *126*, 7460-7461.
(61) Shintani, R.; Otomo, H.; Ota, K.; Hayashi, T. Palladium-Catalyzed Asymmetric Synthesis of Silicon-Stereogenic Dibenzosiloles via Enantioselective C–H Bond Functionalization. *J. Am. Chem. Soc.* **2012**, *134*, 7305-7308.
(62) Tsuda, T.; Choi, S.-M.; Shintani, R. Palladium-Catalyzed Synthesis of Dibenzosilepin Derivatives via 1,n-Palladium Migration Coupled with anti-Carbopalladation of Alkyne. *J. Am. Chem. Soc.* **2021**, *143*, 1641-1650.
(63) Li, P.; Li, Q.; Weng, H.; Diao, J.; Yao, H.; Lin, A. Intramolecular Remote C–H Activation via Sequential 1,4-Palladium Migration To Access Fused Polycycles. *Org. Lett.* **2019**, *21*, 6765-6769.
(64) Ma, S.; Gu, Z. 1,4-Migration of Rhodium and Palladium in Catalytic Organometallic Reactions. *Angew. Chem. Int. Ed.* **2005**, *44*, 7512-7517.
(65) Campo, M. A.; Larock, R. C. Novel 1,4-Palladium Migration in Organopalladium Intermediates Derived from o-Iodobiaryls. *J. Am. Chem. Soc.* **2002**, *124*, 14326-14327.
(66) Karig, G.; Moon, M.-T.; Thasana, N.; Gallagher, T. C–H Activation and Palladium Migration within Biaryls under Heck Reaction Conditions. *Org. Lett.* **2002**, *4*, 3115-3118.
(67) Campo, M. A.; Zhang, H.; Yao, T.; Ibdah, A.; McCulla, R. D.; Huang, Q.; Zhao, J.; Jenks, W. S.; Larock, R. C. Aryl to Aryl Palladium Migration in the Heck and Suzuki Coupling of o-Halobiaryls. *J. Am. Chem. Soc.* **2007**, *129*, 6298-6307.
(68) Campo, M. A.; Huang, Q.; Yao, T.; Tian, Q.; Larock, R. C. 1,4-Palladium Migration via C–H Activation, Followed by Arylation: Synthesis of Fused Polycycles. *J. Am. Chem. Soc.* **2003**, *125*, 11506-11507.
(69) Bhunia, S. K.; Polley, A.; Natarajan, R.; Jana, R. Through-Space 1,4-Palladium Migration and 1,2-Aryl Shift: Direct Access to Dibenzo[a,c]carbazoles through a Triple C-H Functionalization Cascade. *Chem. Eur. J.* **2015**, *21*, 16786-16791.
(70) Singh, A.; Sharp, P. R. Pt and Pd 1,4-Shifts at the Edge of Dibenz[a,c]anthracene. *J. Am. Chem. Soc.* **2006**, *128*, 5998-5999.
(71) Full, J.; Panchal, S. P.; Götz, J.; Krause, A.-M.; Nowak-Król, A. Modular Synthesis of Organoboron Helically Chiral Compounds: Cutouts from Extended Helices. *Angew. Chem. Int. Ed.* **2021**, *60*, 4350-4357.
(72) Song, S.; Huang, G.; Kojima, T.; Nakae, T.; Uno, H.; Sakaguchi, H. Interchain-linked Graphene Nanoribbons from Dibenzo[*g*,*p*]chrysene via Two-zone Chemical Vapor Deposition. *Chem. Lett.* **2017**, *46*, 1525-1527.
(73) Fujii, Y.; Taguchi, Y.; Tokai, S.; Matsumoto, Y.; Yoshida, N.; Iwasawa, T. Relevant analysis to the productivity in selective synthesis of dibenzo[g,p]chrysene derivatives. *Tetrahedron* **2021**, *95*, 132353.
(74) Cook, X. A. F.; de Gombert, A.; McKnight, J.; Pantaine, L. R. E.; Willis, M. C. The 2-Pyridyl Problem: Challenging Nucleophiles in Cross-Coupling Arylations. *Angew. Chem. Int. Ed.* **2021**, *60*, 11068-11091.
(75) Full, F.; Wölflick, Q.; Radacki, K.; Braunschweig, H.; Nowak-Król, A. Enhanced Optical Properties of Azaborole Helicenes by Lateral and Helical Extension. *Chem. Eur. J.* **2022**, *28*, e202202280.
(76) Full, F.; Wildervanck, M. J.; Volland, D.; Nowak-Król, A. Synthesis of Enantioenriched Azaborole Helicenes by Chirality Transfer from Axially Chiral Biaryls. *Synlett* **2023**, *34*, 477-482.
(77) Volland, D.; Niedens, J.; Geppert, P. T.; Wildervanck, M. J.; Full, F.; Nowak-Król, A. Synthesis of a Blue-Emissive Azaborathia[9]helicene by Silicon-Boron Exchange from Unusual Atropisomeric Teraryls. *Angew. Chem. Int. Ed.* **2023**, *62*, e202304291.
(78) Full, J.; Wildervanck, M. J.; Dillmann, C.; Panchal, S. P.; Volland, D.; Full, F.; Meerholz, K.; Nowak-Król, A. Impact of Truncation on Optoelectronic Properties of Azaborole Helicenes. *Chem. Eur. J.* **2023**, *29*, e202302808.

(79) Noteworthy, we detected only traces of other compounds that have not been further characterized.
(80) Chai, J.-D.; Head-Gordon, M. Long-Range Corrected Hybrid Density Functionals with Damped Atom–Atom Dispersion Corrections. *Phys. Chem. Chem. Phys.* **2008**, *10*, 6615-6620.
(81) Weigend, F. Accurate Coulomb-Fitting Basis Sets for H to Rn. *Phys. Chem. Chem. Phys.* **2006**, *8*, 1057-1065.
(82) Weigend, F.; Ahlrichs, R. Balanced Basis Sets of Split Valence, Triple Zeta Valence and Quadruple Zeta Valence Quality for H to Rn: Design and Assessment of Accuracy. *Phys. Chem. Chem. Phys.* **2005**, *7*, 3297-3305.
(83) Valadbeigi, Y. Organometallic acids with azaborine, oxaborine, azaborole and oxaborole scaffolds. *New J. Chem.* **2018**, *42*, 18777-18786.
(84) Dixit, V. A.; Goundry, W. R. F.; Tomasi, S. C=C/B–N substitution in five membered heterocycles. A computational analysis. *New J. Chem.* **2017**, *41*, 3619-3633.
(85) Artigas, A.; Hagebaum-Reignier, D.; Carissan, Y.; Coquerel, Y. Visualizing electron delocalization in contorted polycyclic aromatic hydrocarbons. *Chem. Sci.* **2021**, *12*, 13092-13100.
(86) Szczepanik, D. W.; Andrzejak, M.; Dominikowska, J.; Pawełek, B.; Krygowski, T. M.; Szatylowicz, H.; Solà, M. The electron density of delocalized bonds (EDDB) applied for quantifying aromaticity. *Phys. Chem. Chem. Phys.* **2017**, *19*, 28970-28981.
(87) Jimenez-Halla, J. O. C.; Matito, E.; Solà, M.; Braunschweig, H.; Hörl, C.; Krummenacher, I.; Wahler, J. A theoretical study of the aromaticity in neutral and anionic borole compounds. *Dalton Transactions* **2015**, *44*, 6740-6747.
(88) Iida, A.; Sekioka, A.; Yamaguchi, S. Heteroarene-fused boroles: what governs the antiaromaticity and Lewis acidity of the borole skeleton? *Chem. Sci.* **2012**, *3*, 1461-1466.
(89) Clar, E., *The Aromatic sextet*. Wiley: London, 1972.
(90) Solà, M. Forty years of Clar's aromatic π-sextet rule. *Front. Chem.* **2013**, *1*, 22.